PAPER • OPEN ACCESS

Density pedestal prediction model for tokamak plasmas

To cite this article: S. Saarelma *et al* 2024 *Nucl. Fusion* **64** 076025

OPEN ACCESS
IOP Publishing | International Atomic Energy Agency
Nuclear Fusion
Nucl. Fusion **64** (2024) 076025 (9pp)
https://doi.org/10.1088/1741-4326/ad4b3e

Density pedestal prediction model for tokamak plasmas

S. Saarelma[1,*], J.W. Connor[1], P. Bílková[2], P. Bohm[2], C. Bowman[1], A.R. Field[1], L. Frassinetti[3], R. Friedström[3], S. Henderson[1], K. Imada[4], A. Kirk[1], O.J. Kwon[5], T. Luda[6], R. Sarwar[1], R. Scannell[1], S.F. Smith[1], the ASDEX Upgrade Team[4,a], MAST-U team[1], STEP team[1], JET Contributors[b] and the Eurofusion Tokamak Exploitation Team[c]

[1] United Kingdom Atomic Energy Authority, Culham Campus, Abingdon OX14 3DB, United Kingdom of Great Britain and Northern Ireland
[2] Institute of Plasma Physics of the CAS, Za Slovankou 3, 182 00 Prague 8, Czech Republic
[3] Division of Fusion Plasma Physics, KTH Royal Institute of Technology, Stockholm SE-100 44, Sweden
[4] York Plasma Institute, University of York, Heslington, York YO10 5DD, United Kingdom of Great Britain and Northern Ireland
[5] Department of Physics, Daegu University, Gyungbuk, Korea, Republic Of
[6] Max–Planck–Institut für Plasmaphysik, Boltzmannstrasse 2, D–85748 Garching, Germany

E-mail: samuli.saarelma@ukaea.uk

Received 18 January 2024, revised 16 April 2024
Accepted for publication 14 May 2024
Published 3 June 2024

Abstract

A model for the pedestal density prediction based on neutral penetration combined with pedestal transport is presented. The model is tested against a pedestal database of JET-ILW Type I ELMy H-modes showing good agreement over a wide range of parameters both in standalone modelling (using the experimental temperature profile) and in full Europed modelling that predicts both density and temperature pedestals simultaneously. The model is further tested for ASDEX Upgrade and MAST-U Type I ELMy H-modes and both are found to agree with the same model parameters as for JET-ILW. The JET-ILW experiment where the isotope of the main ion is varied in a D/T scan at constant gas rate and constant β_N is successfully modelled as long as the separatrix density ($n_{e,sep}$) and pedestal transport coefficient ratio (D/χ) are varied in accordance with the experimentally observed variation of $n_{e,sep}$ and the isotope dependence of D/χ found in gyrokinetic simulations. The predictions are found to be sensitive to $n_{e,sep}$ which is why the model is combined with an $n_{e,sep}$ model to predict the pedestal for the STEP fusion reactor.

Keywords: pedestal density, prediction, H-mode, tokamak

(Some figures may appear in colour only in the online journal)

[a] See Zohm *et al* 2024 (https://doi.org/10.1088/1741-4326/ad249d) for the ASDEX Upgrade Team.
[b] See Maggi *et al* 2024 (https://doi.org/10.1088/1741-4326/ad3e16) for JET Contributors.
[c] See Joffrin *et al* 2024 (https://doi.org/10.1088/1741-4326/ad2be4) for the EUROfusion Tokamak Exploitation Team.
[*] Author to whom any correspondence should be addressed.

1. Introduction

To maximize the efficiency of a tokamak based fusion reactor the confinement of the plasma should be optimized. The main operating regime with good confinement is the so called high confinement mode or H-mode in which a transport barrier near the plasma edge develops a steep pressure gradient region called the pedestal. Since the temperature gradient in the core plasma is often 'stiff' due to turbulence that clamps $\nabla T/T$ close to a threshold value [1], the global confinement of the tokamak can be optimized by increasing the height of the pedestal temperature. Thus, a reliable model for the pedestal is a key requirement for predicting the performance of burning plasma devices, such as ITER [2] or the proposed spherical tokamak STEP [3].

The EPED model [4, 5] is based on the requirement that the pedestal plasma pressure profile is marginally stable to both kinetic ballooning modes (KBMs) and peeling-ballooning modes. While the EPED model has had great success in predicting the pressure pedestal on existing tokamaks it is not able to separately predict density and temperature pedestals but instead takes the density pedestal as an input to the model. In order to be fully predictive, the EPED model has to be extended to include the prediction of the density pedestal along with the temperature pedestal.

A model based on a combination of neutral particles ionisation, charge exchange and plasma particle transport to predict the density pedestal structure is introduced in [6]. In [6] the free parameters related to the transport coefficients in the model are set based on the experimental JET data and it is validated for the JET-ILW (ITER-like beryllium–tungsten wall) database [7] with good results. Here we introduce the model shortly in section 2. In section 3 we expand the validation effort to two other tokamaks, ASDEX Upgrade and MAST-U. The pedestal density is predicted in two ways: using the experimental temperature profiles as input and predicting the temperature profile with the EPED1 model [4] together with the density prediction. After the validation, in section 4 we discuss the sensitivity of the prediction to the boundary condition used, namely the separatrix density. We combine the pedestal density model with a model that predicts the separatrix density to predict the JET density pedestals using only engineering parameters in the model. In section 5 we address a particular effect on the pedestal density, namely the isotope effect, by testing a dedicated scan of the isotope mass of the plasma ions on JET. Finally in section 6, we use the model to predict the pedestal density of the STEP fusion reactor and discuss the sensitivity of the prediction.

2. Density prediction model

In the model by Groebner *et al* [8], which further develops the model by Mahdavi *et al* [9], the neutral particles from outside the separatrix are assumed to be freely streaming at the dissociation or so-called Franck–Condon energy. The increase of plasma density through ionisation in the edge plasma is compensated by diffusive plasma transport until a steady state is reached where the ionisation and the transport are in balance. This model ignores the charge exchange processes that can increase the energy of the neutral particles, allowing them to reach further into the plasma before getting ionised. Burrell's model [10] treats neutral penetration as a diffusive process but includes the charge exchange neutrals into the model. Interestingly, this leads to an analytic solution for the neutral density having the same functional form as that for the free streaming model, although the resulting neutral penetration depth, λ, is different. Furthermore, in the pedestal temperature range 40–200 eV, the numerical values of the corresponding values of λ are rather similar. The diffusion model becomes valid when $\sigma_{\mathrm{CX}} v_{\mathrm{th,i}} \gg \sigma_{\mathrm{i}} v_{\mathrm{th,e}}$ (σ_{CX} and σ_{i} are charge exchange and ionisation cross sections, respectively, and $v_{\mathrm{th,i}}$ and $v_{\mathrm{th,e}}$ are the thermal velocities of ions and electrons, respectively) [11], which is appropriate for higher pedestal temperatures, say, around 1 keV, when the predicted value of λ for the free streaming model would greatly exceed that for the diffusion model. The model presented below does involve free streaming of both Franck–Condon and charge exchange neutrals.

In our model we obtain the radial profile of the electron density, $n_{\mathrm{e}}(r)$, in the H-mode pedestal region by balancing radial diffusion, with coefficient $D_{\mathrm{ped}}(r)$, against ionisation of both low energy Franck–Condon and the more energetic charge exchange neutrals, with densities $n_{\mathrm{FC}}(r)$ and $n_{\mathrm{CX}}(r)$, respectively, themselves being modelled by balancing inward convection against ionisation and charge exchange sources and sinks.

The ionisation model described above is represented by the three equations:

$$\nabla.(D_{\mathrm{ped}} \nabla n_{\mathrm{e}}) = -n_{\mathrm{e}} (n_{\mathrm{FC}} + n_{\mathrm{CX}}) S_{\mathrm{i}} \tag{1}$$

$$\nabla.(V_{\mathrm{FC}} n_{\mathrm{FC}}) = -n_{\mathrm{e}} (n_{\mathrm{FC}} S_{\mathrm{i}} + n_{\mathrm{FC}} S_{\mathrm{CX}}) \tag{2}$$

$$\nabla.((V_{\mathrm{CX}} n_{\mathrm{CX}})) = -n_{\mathrm{e}} \left(n_{\mathrm{CX}} S_{\mathrm{i}} - \frac{1}{2} n_{\mathrm{FC}} S_{\mathrm{CX}} \right), \tag{3}$$

where S_{i} and S_{CX} are the ionisation and charge exchange rates, respectively, while V_{FC} and V_{CX} are the corresponding radial velocities of the two species, each considered to be mono-energetic. Strictly speaking S_{i} and S_{CX} depend on temperature and density but since the main dependency is on temperature [12], for simplicity we assume here that they depend only on temperature. Thus, $S_{\mathrm{i}} = \sigma_{\mathrm{i}} v_{\mathrm{th,e}}$, $S_{\mathrm{CX}} = \sigma_{\mathrm{CX}} v_{\mathrm{th,i}}$. The diffusion coefficient D_{ped} may have a radial profile and this is explained more in detail below. For the radial velocities of the neutrals, we follow [13], setting $|V_{\mathrm{FC},r}| = \sqrt{8E_{\mathrm{FC}}/\pi^2 M_{\mathrm{i}}}$, with $E_{\mathrm{FC}} \sim 3$ eV, and $|V_{\mathrm{CX},r}| = \sqrt{2T_{\mathrm{i}}/\pi M_{\mathrm{i}}}$ (we drop the suffix r, below). The factor $1/2$ in equation (3) represents the fact that the outward flux of fast charge exchange neutrals is taken to be lost.

The derivation of the model is fully described in [6] and here we present only the final one dimensional differential equation to be solved:

$$\frac{\mathrm{d}}{\mathrm{d}x}\left(\left\langle|\nabla r|^2\right\rangle D_{\mathrm{ped}}\frac{\mathrm{d}n_{\mathrm{e}}}{\mathrm{d}x}\right) = n_{\mathrm{e}}S_{\mathrm{i}}\left[\frac{(S_{\mathrm{i}}+S_{\mathrm{CX}})}{(S_{\mathrm{i}}+S_{\mathrm{CX}}/2)}\frac{\left\langle|\nabla r|^2\right\rangle D_{\mathrm{ped}}}{|V_{\mathrm{FC}}|f_{\mathrm{FC}}}\frac{\mathrm{d}n_{\mathrm{e}}}{\mathrm{d}x} - \frac{(S_{\mathrm{i}}+S_{\mathrm{CX}})}{\left(S_{\mathrm{i}}+\frac{S_{\mathrm{CX}}}{2}\right)} \times \frac{C}{|V_{\mathrm{FC}}|f_{\mathrm{FC}}} + \left(\frac{(S_{\mathrm{i}}+S_{\mathrm{CX}})}{(S_{\mathrm{i}}+S_{\mathrm{CX}}/2)}\frac{|V_{\mathrm{CX}}|f_{\mathrm{CX}}}{|V_{\mathrm{FC}}|f_{\mathrm{FC}}}-1\right)\langle n_{\mathrm{CX}}\rangle\right] \tag{4}$$

$$\langle n_{\mathrm{CX}}\rangle = \langle n_{\mathrm{CX}}(0)\rangle \exp\left(\int_0^x \mathrm{d}x' \frac{n_{\mathrm{e}}(x')S_{\mathrm{i}}}{[V_{\mathrm{CX}}]f_{\mathrm{CX}}}\right) + \frac{|V_{\mathrm{FC}}|f_{\mathrm{FC}}S_{\mathrm{CX}}\langle n_{\mathrm{FC}}(0)\rangle}{2[V_{\mathrm{CX}}]f_{\mathrm{CX}}\left(S_{\mathrm{i}}+S_{\mathrm{CX}}-\frac{|V_{\mathrm{FC}}|f_{\mathrm{FC}}}{V_{\mathrm{CX}}f_{\mathrm{CX}}}S_{\mathrm{i}}\right)}. \tag{5}$$

Here $<>$ refers to the flux surface average. x is a radial coordinate with the origin corresponding to the separatrix. f_{CX} and f_{FC} are form factors for charge exchange and Franck–Condon neutrals. They account for the poloidal distribution of the respective neutral populations. Even though there is evidence of poloidal asymmetry of the sources [14], for simplicity, in this work both have been set to 1 but can be adjusted if more information on the poloidal neutral particle distribution is available. One thing to note is that the modelling in section 3 was done with a fixed value of $\langle n_{\mathrm{FC}}(0)\rangle$ for all shots. Having a slightly higher value of $\langle n_{\mathrm{FC}}(0)\rangle$ and f_{CX} and f_{FC} below 1 (which is expected if neutrals are more concentrated near the X-point) would lead to results very similar to those shown. In any case, if a more comprehensive model for the scrape-off layer is integrated with our simple model, the uncertainties related to these quantities can be reduced. c is a constant of integration from integrating equation (1) and is defined as $c = \langle|\nabla r|^2\rangle D_{\mathrm{ped}}\frac{\mathrm{d}n_{\mathrm{e}}}{\mathrm{d}x}|_{x=-\infty}$, where $\frac{\mathrm{d}n_{\mathrm{e}}}{\mathrm{d}x}|_{x=-\infty}$ is the electron density gradient in the core representing the particle flux from the core. Finally, D_{ped} is the particle diffusion coefficient in the pedestal region. We will describe next how it is determined.

Following [15] we assume that the particle diffusion in the pedestal region is a combination of the neoclassical and turbulent fluxes. The turbulent flux is divided into two components, that due to KBM, which is driven by the pressure gradient once a threshold value of the gradient is exceeded and that due to temperature gradient or TG driven turbulence. Even though we here use the term 'TG', this part of the particle flux is taken to represent all the turbulence driven by the temperature gradient, not only the modes that are described in gyrokinetic simulations (such as in [16]) as 'ITG modes' or 'ETG modes'. For this model, the character of turbulence is not important, only the driving gradient. The combined particle diffusion coefficient is then $D_{\mathrm{ped}} = D_{\mathrm{KBM}} + D_{\mathrm{TG}} + D_{\mathrm{NEO}}$

$$D_{\mathrm{NEO}} = \frac{\chi_{\mathrm{NEO}}}{2} = 0.05\left(\frac{\rho_{\mathrm{s}}^2 c_{\mathrm{s}}}{a}\right) \tag{6}$$

$$D_{\mathrm{TG}} = \left(\frac{D}{\chi}\right)_{\mathrm{TG}}\frac{P_{\mathrm{tot,e}}}{Sn_{\mathrm{e}}\nabla \mathrm{T}} \tag{7}$$

$$D_{\mathrm{KBM}} = \begin{cases} C_{\mathrm{KBM}}(\alpha-\alpha_{\mathrm{crit}})\cdot\left(\frac{\rho_{\mathrm{s}}^2 c_{\mathrm{s}}}{a}\right), \alpha > \alpha_{\mathrm{crit}} \\ 0, \alpha < \alpha_{\mathrm{crit}} \end{cases}, \tag{8}$$

$$\text{With } \alpha = \frac{2\mathrm{d}V/\mathrm{d}\psi}{(2\pi)^2}\left(\frac{V}{2\pi^2 R_0}\right)^{1/2}\mu_0\frac{\mathrm{d}p}{\mathrm{d}\psi}. \tag{9}$$

Here ρ_{s} is the ion Larmor radius, c_{s} is the ion sound speed, a is the tokamak minor radius, $P_{\mathrm{tot,e}}/S$ is the total power flux carried by electrons through the pedestal, α is the normalised pressure gradient, V is the plasma volume, ψ is the poloidal flux, R_0 is the geometric centre of the plasma and p is the pressure. The terms $\left(\frac{D}{\chi}\right)_{\mathrm{TG}}$, C_{KBM} and α_{crit} are adjustable parameters in the model. $\left(\frac{D}{\chi}\right)_{\mathrm{TG}}$ represents the ratio of particle to electron heat flux due to the temperature gradient driven turbulence, C_{KBM} represents the strength of the KBM turbulence when the pressure gradient threshold α_{crit} is exceeded.

In addition, the ordinary differential equations (4) and (5) require boundary conditions to solve them. The separatrix density, $n_{\mathrm{e,sep}}$ is taken from the experiment by defining it at the same radial location as where the separatrix temperature is given by the 2-point model [17]. In section 4, we also use a model from [18] to calculate it from engineering parameters. The density gradient at the separatrix is set to $\frac{\mathrm{d}n_{\mathrm{e}}}{\mathrm{d}x}|_{x=0} = -\frac{n_{\mathrm{e}}(0)}{\sqrt{D_{\mathrm{SOL}}\tau_{||}}}$, where the particle diffusion coefficient D_{SOL}, is calculated from equations (6)–(9) at the separatrix and $\tau_{||}$ is the time-scale of free streaming particles along the field lines to the divertor. Finally, the neutral particle density at the separatrix $\langle n_{\mathrm{FC}}(0)\rangle$, and the ratio of Franck–Condon and charge exchange particle densities at the separatrix have to be specified. The sensitivity of the model to these boundary conditions is discussed later, as well as how to include a physical model for them.

In addition to using the experimental value for the separatrix density $n_{\mathrm{e}}(0)$, which is not an engineering parameter (i.e. is not known prior to the experiment), we also tested a 2-point scrape-off layer model based on [18] to predict $n_{\mathrm{e}}(0)$. The model in [18] requires the neutral pressure in the subdivertor region as input. Since that is not an engineering parameter either, we use the total gas injection rate as a proxy to it.

3. Model testing against experiments

The model described above is implemented as a standalone code that uses known experimental pedestal temperature profiles and only predicts the pedestal density and also in Europed [19], where it is combined with the EPED1 model [4] and allows simultaneous prediction of both the density and temperature pedestals. Since the comparison with JET experiments has been presented earlier in [6], we summarise the result here but concentrate on the testing of the model using the parameters found for JET-IL with the experimental data from ASDEX Upgrade (AUG) and MAST-U. The quantity compared between the model simulations, $n_{\mathrm{e,ped}}$ is defined as the density value at $\psi_{\mathrm{N}} = 0.85$. This is also where $\frac{\mathrm{d}n_{\mathrm{e}}}{\mathrm{d}x}|_{x=-\infty}$ needed for the parameter c is defined. Also, by being well inside of the pedestal region, we avoid issues related to different pedestal widths between cases and the fact that the

model does not assume any functional form (such as hyperbolic tangent that is used to fit the experimental data) for density.

3.1. JET

For testing the model against JET type I ELMy H-modes, we use over 1000 discharges from the JET-ILW pedestal database [7], excluding discharges with pellets, RMP ELM mitigation or impurity injection. The plasma parameters in the database cover a wide range: total plasma current $I_p = 1.4$–4.0 MA, toroidal magnetic field $B_t = 1.0$–3.8 T, total heating power $P_{tot} = 3$–31 MW and triangularity $\delta = 0.15$–0.45. The parameters used in both Europed and the standalone model are the following: $\langle n_{FC}(0)\rangle = 10^{15}$ m^{-3} and $\tau_{||} = 0.001$ s which are both reasonable values for JET, and $\alpha_{crit} = 2$ which is slightly below the $n = \infty$ ideal MHD ballooning mode stability limit for JET pedestals and which is where the KBM stability threshold is expected to lie. The ratio $\left(\frac{D}{\chi}\right)_{TG}$ and C_{KBM} were varied to find values that best fit the data. In the standalone modelling using the experimental temperature profile, $\left(\frac{D}{\chi}\right)_{TG} = 0.1$ and $C_{KBM} = 0.3$ were found to give a very good match with the experimental density pedestals (root mean square error, RMSE =15%). We note here that the good match with experiment is not very sensitive to the parameter values as is shown below for a very different set of parameters. The parameter values are also unlikely to be the same in all plasma conditions and our simple assumption to keep them fixed is likely to have contributed to the spread of modelled data. If the simple equations (8)–(10) for pedestal particle diffusivity can be replaced by for instance a reduced transport model based on gyrokinetic simulations, the accuracy of the prediction model is likely to improve further.

In the self-consistent Europed simulations that impose the EPED1 KBM constraint ($\Delta = 0.076\sqrt{\beta_{p,ped}}$, where Δ is the pressure pedestal width and $\beta_{p,ped}$ is the poloidal β at the pedestal top) and predict both the temperature and density pedestals simultaneously, the KBM part in equation (8) in the pedestal density prediction model can often lead to a feedback loop. If the hypothetical pedestal pressure gradient for a given pedestal width exceeds α_{crit} it results in an increased value of D_{ped}, which in turn lowers the density pedestal bringing the pressure gradient closer to the critical value. Europed then forces the pedestal pressure to fulfil the EPED1 condition, which means increased $T_{e,ped}$. This in turn increases the pressure gradient and the loop continues. Replacing the EPED1 condition in Europed with some other pedestal model (e.g. [20]) could possibly avoid this problem. Here, we just set C_{KBM} to zero and increase $\left(\frac{D}{\chi}\right)_{TG}$ to 0.5 to also account for the rest of the KBM turbulence as in this way we avoid the feedback loop.

With these values Europed predicts the density pedestals with an RMSE = 19% which is similar to that achieved using EPED1 for just the pressure pedestal [5]. Figure 1 shows that both methods, Europed and the standalone model, predict the JET pedestal densities over a wide set of pedestals although the accuracy of the standalone model is degraded when the KBM transport is ignored (RMSE = 20%).

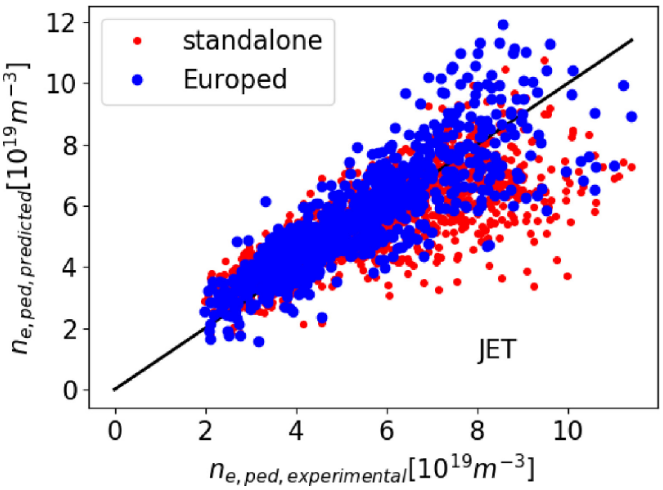

Figure 1. The predicted density pedestal height vs. the experimental density pedestal height for the JET database using the standalone model (red) and full Europed modelling (blue) with the parameters set as $C_{KBM} = 0.0$ and $\left(\frac{D}{\chi}\right)_{TG} = 0.5$.

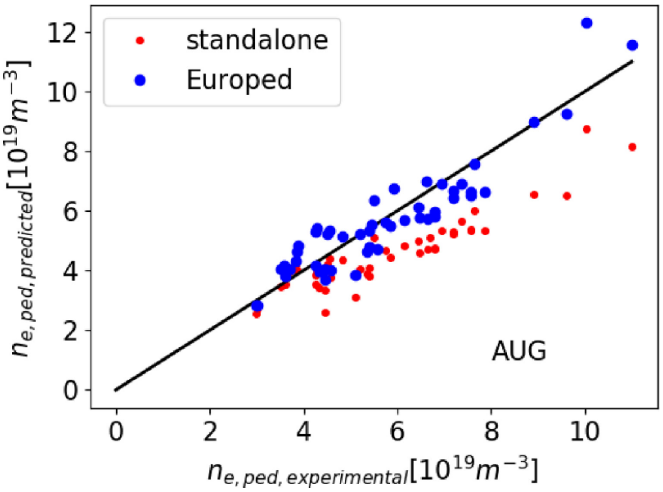

Figure 2. The predicted density pedestal height vs. the experimental density pedestal height for the AUG database using the standalone model (red) and the full Europed modelling (blue) with parameters set at $C_{KBM} = 0.0$ and $\left(\frac{D}{\chi}\right)_{TG} = 0.5$.

3.2. ASDEX Upgrade

The model is tested against an AUG database of 50 discharges that was used in [21], using exactly the same model parameters as were used above for JET ($\left(\frac{D}{\chi}\right)_{TG} = 0.5$, $C_{KBM} = 0$, $\langle n_{FC}(0)\rangle = 10^{15}$ m^{-3} and $\tau_{||} = 0.001$ s). The plasma parameters in the database vary as follows: $I_p = 0.6$–1.2 MA, $B_t = 1.5$–2.9 T, $\delta = 0$–0.35, $P_{tot} = 1.6$–9.8 MW. The comparison with the experiment is shown in figure 2. In this case the RMSE is 13% for Europed (with 0.09 used as the width constraint

as AUG has reported having wider pedestals than which the standard EPED1 scaling assumes [22]) and 21% for the standalone model. The agreement with the experimental density data is remarkably good for Europed considering that we used the same parameters that were found to work for JET without any adjustments. Also, the temperature pedestal is predicted very well, with an RMSE = 16%.

The standalone model works acceptably at low density but significantly under-predicts the experimental data at higher densities for which the reason is not clear. One possible explanation is that the experimental temperature gradient at high density is shallower than that predicted by Europed. This would lead to a higher value of χ_{TG} (see equation (7)), which would then increase D_{ped}. The Europed model predicts steeper temperature gradients, leading to lower D_{ped} and hence higher density. The experimental measurements on ASDEX Upgrade confirm that D_{ped} and χ_{e} should be related as is done in the model, and also that a pinch term (that the model discussed here ignores) is not required to explain the experimental data [23].

Finally, if the ASDEX Upgrade pedestals are run with the standalone model using the parameters that were found the best for JET standalone model ($\left(\frac{D}{\chi}\right)_{\mathrm{TG}} = 0.1$, $C_{\mathrm{KBM}} = 0.3$) we obtain very good match with the experiment (RMSE = 15%).

3.3. MAST-U

Since MAST-U has operated only for a short time, the number of shots available for experimental comparison is relatively small compared to that from JET and AUG. In particular, the parameter range used in the experiment is relatively small, since all type I ELMy H-mode experiments have used 750 kA plasma current and the double null plasma shape. This of course limits the range of densities obtained. Furthermore, since MAST-U does not have a cryopump, the line averaged density does not usually saturate during the H-mode phase of the discharge. However, the diagnostic (Thomson scattering, details in [24]) for measuring the density and temperature has a high radial and temporal resolution, which allows sufficiently accurate fitting of profiles even from a single ELM cycle. The modelled and measured density pedestal values are shown in figure 3. As in AUG, the same model parameters as were used to fit JET data were used. In the Europed modelling a KBM width constant of 0.1 was used instead of the standard 0.076 of EPED1. The value of this constant was chosen based on the analysis of MAST data [25].

3.4. Standalone model with realistic parameters

As explained earlier, the KBM constraint in the EPED model when used together with the pedestal density prediction model that includes the KBM transport can result in a feedback loop that leads to a very low density prediction. In practice this can be avoided in Europed by including all KBM driven transport in the turbulent (D_{TG}) term. While this makes $D_{\mathrm{TG}}/\chi_{\mathrm{TG}}$ unphysically large, the predictions agree with the experiment relatively well.

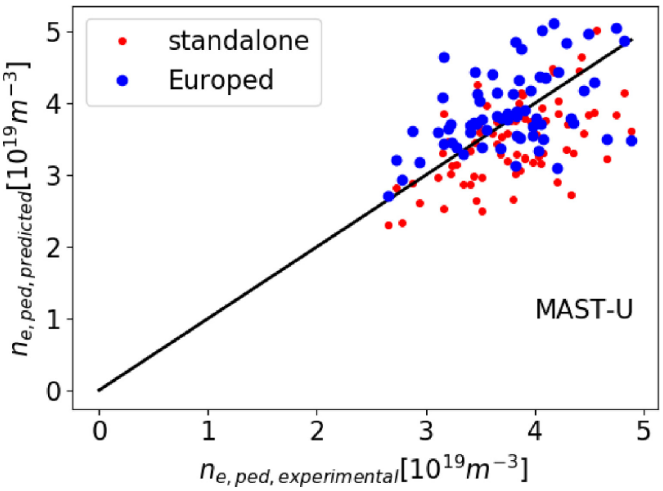

Figure 3. The predicted density pedestal height vs. the experimental density pedestal height for the MAST-U database using the standalone model (red) and the full Europed modelling (blue) with the parameters set at $C_{\mathrm{KBM}} = 0.0$ and $\left(\frac{D}{\chi}\right)_{\mathrm{TG}} = 0.5$.

However, to test the physics assumptions of the density prediction model, we can ignore the temperature pedestal prediction using the EPED model and validate the density model alone with realistic parameters and using the experimental temperature profile. In this test, we use a much lower and a more realistic value: $\left(\frac{D}{\chi}\right)_{TG} = 0.05$ (a typical value for ETG turbulence [26]), together with $C_{\mathrm{KBM}} = 1$ and $\alpha_{\mathrm{crit}} = 2$ for the two convention tokamaks (JET and AUG) and $\alpha_{\mathrm{crit}} = 5$ for the spherical tokamak (MAST-U). The difference in the critical normalised pressure gradient α is in order to take into account the higher ballooning mode stability limit in a spherical tokamak.

With these assumptions we predict the three databases using the standalone model and achieve a very good match with the experiment for all three devices, as shown in figure 4. The RMSE values for the three devices are: 22% (JET), 16% (AUG) and 16% (MAST-U).

This test gives confidence and shows the model can include a substantial KBM component and that allows the other parameters to take physically realistic values. It indicates that while the model struggles with a fully predictive pedestal model that relies on the KBM limit for the pressure gradient (such as EPED), it could work better with a fully predictive model where the explicit pressure gradient constraint is replaced by something else, such as a model for the heat transport through the pedestal.

4. The effect of separatrix density

Since our model has a few parameters that are not necessarily well known *a priori*, and thus need to be set as input, we test its sensitivity to these parameters. The effect of some of the parameters on the prediction was already tested in [6] and it

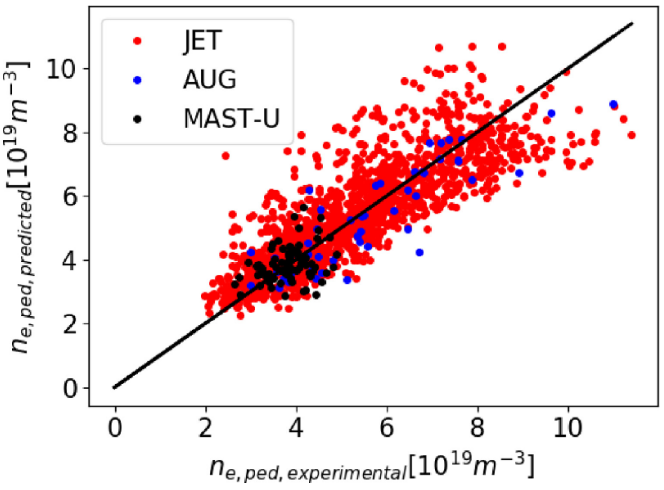

Figure 4. The predicted density pedestal height vs. the experimental density pedestal height for JET (red), AUG (blue) and MAST-U (black) using the standalone model with the parameters set at $C_{\mathrm{KBM}} = 1.0$, $\left(\frac{D}{\chi}\right)_{\mathrm{TG}} = 0.05$ and $\alpha_{\mathrm{crit}} = 2$ (JET and AUG) and $\alpha_{\mathrm{crit}} = 5$ (MAST-U).

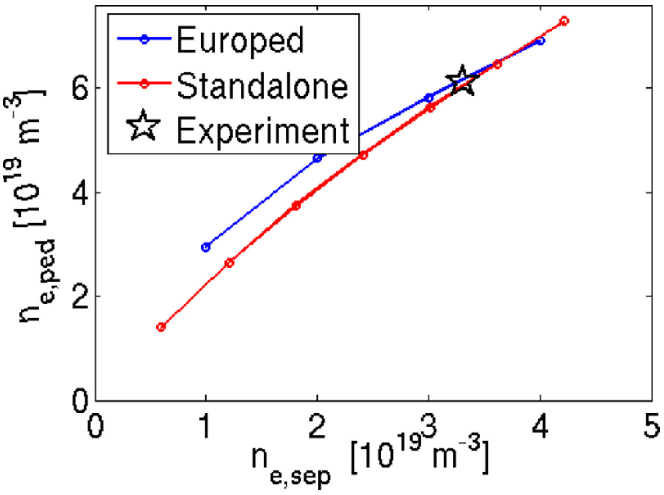

Figure 5. The predicted density pedestal height as a function separatrix density with the standalone model (red) and full Europed model (blue) for a JET discharge 81794. The black star shows the experimental $n_{\mathrm{e,sep}}$ and $n_{\mathrm{e,ped}}$ for this discharge.

was found that the model is relatively robust for instance to the uncertainty of the neutral density at the separatrix. Therefore, we used the same value of $\langle n_{\mathrm{FC}}(0)\rangle = 10^{15}\,\mathrm{m}^{-3}$ for all devices (a reasonable value based on EDGE2D-EIRENE simulations of JET [27]).

However, the sensitivity of the prediction to the separatrix density $n_{\mathrm{e,sep}}$ was identified. In the above modelling we have used the experimental value of $n_{\mathrm{e,sep}}$. However, this is not an engineering parameter, meaning that it is not known prior to the experiment. As can be seen in figure 5, a variation of the input value of $n_{\mathrm{e,sep}}$ in a single JET case produces a significant variation of the predicted pedestal density.

Since $n_{\mathrm{e,sep}}$ is not known before the experiment, this sensitivity leads to a reduced predictive power of the model. However, we can use the model by Kallenbach *et al* [18] to predict $n_{\mathrm{e,sep}}$:

$$n_{\mathrm{e,sep}} = 0.35\frac{2}{e}\left(\frac{2\kappa_0\kappa_z}{7\pi q_{\mathrm{cyl}}}\right)^{\frac{2}{7}}\left(\frac{A_{\mathrm{eff}}}{2}\right)^{0.5}R^{-0.5}\left(\frac{P_{\mathrm{sep}}B}{3\pi\langle\lambda_{\mathrm{HD}}\rangle\langle B_{\mathrm{p}}\rangle}\right)^{\frac{3}{14}} (\gamma\sin(\alpha))^{-0.5}\left(1.5\times10^{23}\mathrm{Pa/(at\,m^{-2}s^{-1})}\right)^{0.5}p_0^{1/4}. \tag{10}$$

The parameters are described in detail in [18] except for A_{eff} that we use to denote the effective isotope mass. Here we note that all the other parameters are known from the equilibrium or are engineering parameters known before the experiment except p_0, which is the divertor neutral pressure. The model has already been successfully used in predictions of AUG [28]. Here we apply it to the JET database and in the modelling use the same dependence between the neutral pressure and gas fuelling and heating power as in [28] for AUG but adjust the scaling coefficient in the formula to fit JET:

$$p_0\,[\mathrm{Pa}] = 0.34\Gamma\left[10^{22}\mathrm{e\,s^{-1}}\right]^{0.67}P_{\mathrm{NBI}}[\mathrm{MW}]^{0.33}. \tag{11}$$

Here Γ is the gas injection rate and P_{NBI} is the total NBI heating power. Figure 6 shows an example case of the experimental and predicted (both standalone and Europed models) as well as the particle diffusion coefficients for the two choices of parameters ($\left(\frac{D}{\chi}\right)_{\mathrm{TG}} = 0.5$, $C_{\mathrm{KBM}} = 0$ and $\left(\frac{D}{\chi}\right)_{\mathrm{TG}} = 0.05$ and $C_{\mathrm{KBM}} = 1$) as well as the radial profiles of Franck–Condon and charge–exchange neutrals. It must be noted that the case (JET discharge #81794) was chosen as in this case the feedback loop described in section 3.4 is not triggered and the Europed prediction works even with a significant C_{KBM}, which is not the case for all the discharges. In this case, also the Europed predicted temperature profile is very close to the experimental profile (not shown), which is of course expected for a case that has very similar predictions with the standalone and the Europed models.

With the modelled $n_{\mathrm{e,sep}}$ and the same parameters of the standalone model as above, the prediction accuracy of the density pedestal is degraded only slightly compared to using the experimental value for the separatrix density (separatrix location determined by the $T_{\mathrm{e,sep}}$ from the 2-point model [17]). This is shown in figure 7. The RMSE of the density prediction is 23%. The RMSE for the predicted $n_{\mathrm{e,sep}}$ compared to the value obtained by the separatrix temperature condition is considerably higher, 36%. This indicates that while the model is sensitive to $n_{\mathrm{e},sep}$, for the purposes of predicting the pedestal density, the separatrix density prediction model is working almost as accurately as determining the experimental separatrix based on the separatrix temperature, and that a part of the scatter in figures 1 and 5 is probably from the inaccurate determination of the separatrix density and not necessarily from the inaccuracy of the prediction model itself. It must be noted here that the results are very similar if the equation (11) is replaced by a formula that has a different dependence on

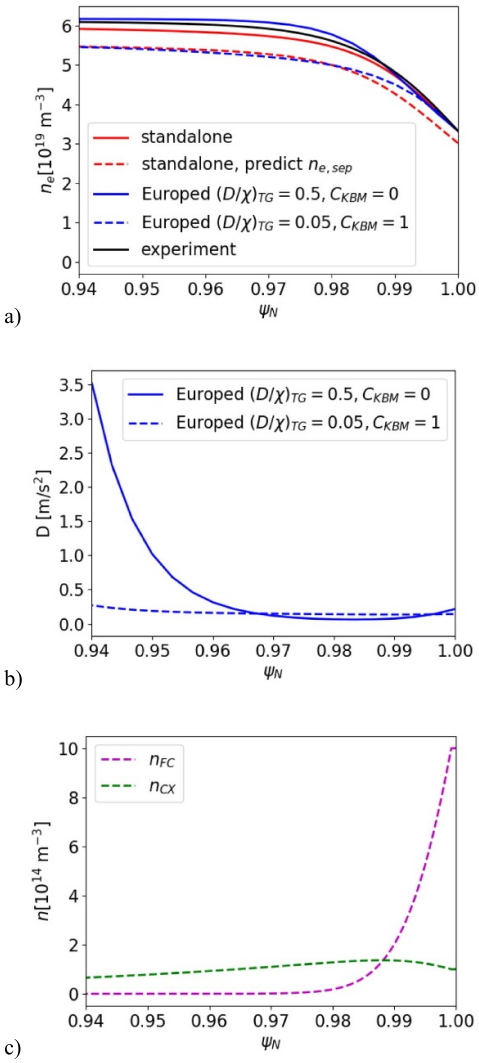

Figure 6. The profiles for an example case of JET #81794 showing the predicted and experimental density profiles (*a*), the particle diffusion coefficients with and without KBM transport in the model (*b*) and the Franck–Condon (n_{FC}) and charge–exchange (n_{CX}) neutral particle densities. The standalone case is run with $\left(\frac{D}{\chi}\right)_{TG} = 0.5$ and $C_{KBM} = 0$ and with the experimental separatrix density and the density predicted using equations (10) and (11).

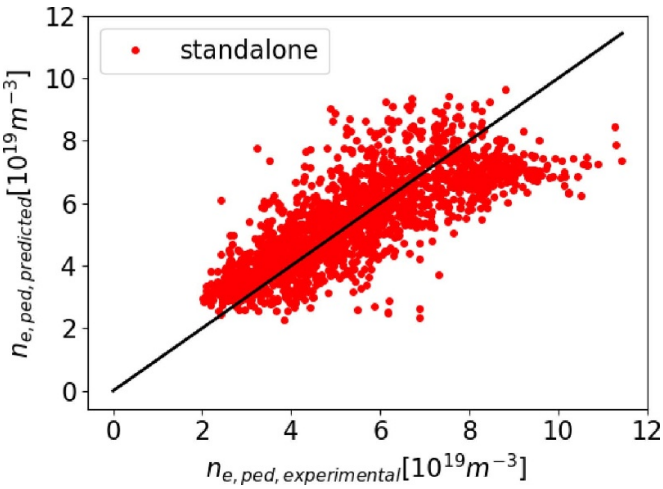

Figure 7. The predicted density pedestal height vs. the experimental density pedestal height for the JET database when the separatrix density is predicted using equations (10) and (11) and the parameters of the density pedestal prediction model are set to $C_{KBM} = 1.0$, $\left(\frac{D}{\chi}\right)_{TG} = 0.05$ and $\alpha_{crit} = 2$.

the gas injection rate ($p_0 \propto \Gamma$) fitted for a small set of JET data in [29]. Separating the data according to the divertor configuration and using a different dependence on the gas rate for each configuration improves the fit slightly. This indicates that the pumping efficiency is different for different divertors as is shown experimentally in [30] and points to the need for scrape-off layer modelling with a code like SOLPS [31] for a truly physics based prediction of $n_{e,sep}$.

5. Dependence on isotope mass

In the JET experiment it has been found that the isotope of the main ion in the plasma affects the pedestal density [32–35]. One would think from a naïve neutral penetration point of view that the plasmas with lighter isotopes would have a higher density pedestal as the neutral particles have higher velocity and penetrate deeper in the plasma than heavier isotopes. This is indeed what the model presented here predicts if one changes only the mass of the main ions and keeps everything else the same. On the contrary, in the experiments it is observed that the density pedestal height increases with increasing isotope mass $A_{eff} = m_i/m_p$. This seems to be an obvious contradiction between the model and the experiment. However, it is not the case that everything else stays fixed when the main ion isotope changes. First, it is observed that the separatrix density also increases with the isotope mass [33], which is also consistent with the $n_{e,sep}$ model described in [18] that predicts the scaling $n_{esep} \sim A_{eff}^{0.5}$. As was shown above, the model predictions are relatively sensitive to this parameter, which means that the separatrix density dependence of the isotope mass propagates through to the pedestal density prediction. Furthermore, in gyrokinetic simulations of H vs D pedestals of JET-ILW, it is found that the increasing isotope mass decreases the D/χ ratio in the pedestal [36]. Together, these effects can overcome the neutral penetration effect and reverse the isotope mass dependency in the pedestal predictions.

We test the combined effect of all three mass dependencies (neutral penetration, separatrix density and particle transport) by modelling an isotope scan experiment from hydrogen to deuterium to tritium and including mixed isotope cases between full deuterium and tritium cases (see [35] for details on the experiment of the D/T ratio scan at constant gas rate and β_N). In the simulation we use the experimental $n_{e,sep}$, assume $D_{KBM} = 0$ and decrease the pedestal $\left(\frac{D}{\chi}\right)_{TG}$ ratio from 1 (hydrogen) to 0.5 (deuterium) and to 0.25 (tritium) which is consistent with the gyrokinetic simulations of [36]. Figure 8 shows how the model predicts the density pedestal through the isotope mass scan. With the combined effects of increasing $n_{e,sep}$ with A_{eff} and the decreasing $\left(\frac{D}{\chi}\right)_{TG}$ with A_{eff} along

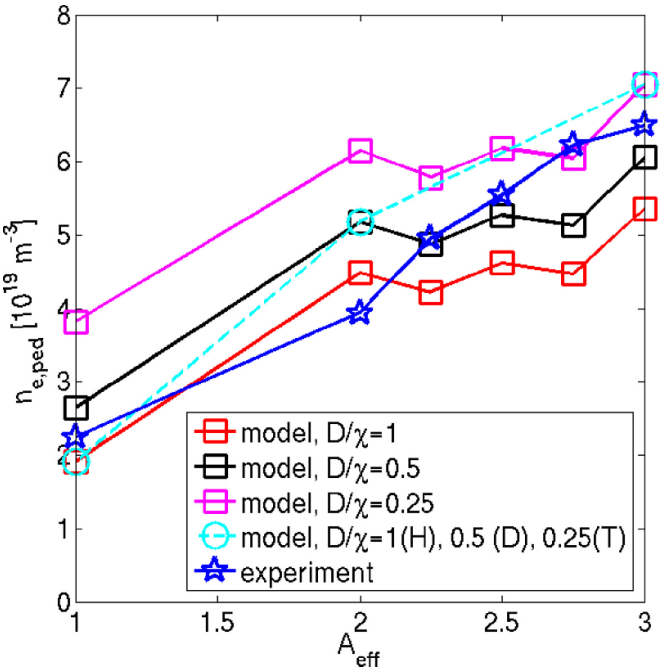

Figure 8. The density pedestal height as a function of the mass of the main ion in the experiment (blue stars) and in three scans with different values of $\left(\frac{D}{\chi}\right)_{TG}$ (red = 1, black = 0.5, magenta = 0.25) and experimental $n_{e,sep}$. The cyan line shows the trend if the $\left(\frac{D}{\chi}\right)_{TG}$ is decreased along with increasing A_{eff}.

with the isotope mass dependence on the neutral penetration, the trend of increasing $n_{e,ped}$ observed in the experiment is well reproduced by the model.

6. Prediction for STEP

STEP is a planned spherical tokamak fusion reactor with the parameters of $R_{geo} \approx 3.6$ m, $A = 1.8$, $I_p \approx 21$ MA, $B_t(R_{geo}) = 3.2$ T, auxiliary power $P_{aux} \approx 150$ MW and $P_{fus} \approx 1.8$ GW. It is planned to operate at high elongation ($\kappa \approx 3$) and normalized β ($\beta_N \approx 4-5$) [35]. We use these parameters and the fully predictive model to predict the density pedestal along with the temperature pedestal in the full Europed model with the same parameters that were used in sections 3.1–3.3 for current devices. With this set of parameters, we obtain $n_{e,ped} = 7 - 10 \times 10^{19} m^{-3}$ and $n_{e,sep} = 3 - 7 \times 10^{19} m^{-3}$ depending on what is assumed for the divertor neutral pressure in the separatrix density model. The assumed range covers different detached divertor solutions with varying amount of impurity radiator. The predicted pedestal densities are slightly higher than what is assumed in the integrated modelling based on the requirements of the exhaust solution [37]. However, since the STEP pedestals are expected to be limited by the peeling modes due to low collisionality, the higher pedestal density leads to higher predicted pedestal pressure, which in turn leads to higher core pressure and fusion power indicating that from the point of view of fusion power projections, the integrated modelling has been performed using conservative assumptions.

7. Discussion and conclusions

The pedestal prediction model based on neutral penetration and transport is applied to JET, AUG and MAST-U Type I ELMy H-modes. The model predicts the density pedestal for all of the devices without adjusting the transport coefficients from the values that were found to work for JET and that are within reasonable agreement with what gyrokinetic theory would predict for turbulent particle transport. In addition, the model is able to reproduce the variation of the pedestal density with the isotope mass when the experimental isotope effect on the separatrix density and the particle transport coefficient variation with isotope mass found in gyrokinetic simulations for the JET-ILW pedestals are correctly taken into account. The largest sensitivity in the model is the strong dependence of the pedestal density on the separatrix density. The separatrix density model of [17, 28] combined with density pedestal model presented in this paper reproduced the experimental JET pedestal density data with equal accuracy as if the separatrix density was determined from the experimental profile data using a 2-point model for the separatrix temperature. Further predictive models will be needed to predict the separatrix density purely from engineering parameters.

The KBM part of the density prediction model and the KBM constraint in the EPED model were found to lead to a feedback mechanism when both the density and the temperature were predicted simultaneously. This forces the model to be used with unphysically high heat flux driven particle transport and without any KBM transport. To be able to use more realistic transport that the density prediction model is able to use in the standalone version, the KBM constraint in the EPED model should be replaced with a model that only constrains the temperature profile as any model that fixes the pressure gradient and uses that to determine the temperature profile is likely to lead to a feedback model.

We recognize that the transport assumption in the model is very simple as it is characterised by only three parameters (α_{crit}, $\left(\frac{D}{\chi}\right)_{TG}$ and C_{KBM} that are considered fixed for all the databases, with the exception of α_{crit} for a spherical tokamak. As such, it is surprising that it is able to predict the pedestal densities for three different devices as well as it can. However, if fast models to evaluate the parameters for individual plasmas are developed, they can easily be incorporated into the model to make it even more accurate. The same applies to the main uncertainty in the model, namely the separatrix density. In this paper, we used the model from [18] but even that has parameters that need to be fitted for each device individually. A true scrape-off layer model that is device independent would be needed to make the predictions of density pedestals truly independent of parameters that are not based on first-principles physics models.

Acknowledgments

This work has been carried out within the framework of the EUROfusion Consortium, funded by the European Union via the Euratom Research and Training Programme (Grant

Agreement No. 101052200—EUROfusion). Views and opinions expressed are however those of the author(s) only and do not necessarily reflect those of the European Union or the European Commission. Neither the European Union nor the European Commission can be held responsible for them. This work has been (part-) funded by the EPSRC Energy Programme (Grant Numbers EP/W006839/1). O.J. Kwon's visit to CCFE was supported by the National R&D Program through the National Research Foundation of Korea (NRF) funded by the Korea government (Ministry of Science and ICT) (NRF-2021M1A7A4091135). This research is part-funded by US Department of Energy, through General Atomics (contract number DE-SC0018990). To obtain further information on the data and models underlying this paper please contact PublicationsManager@ukaea.uk*.

ORCID iDs

S. Saarelma https://orcid.org/0000-0002-6838-2194
J.W. Connor https://orcid.org/0000-0001-9666-6103
P. Bílková https://orcid.org/0000-0002-6156-9773
P. Bohm https://orcid.org/0000-0003-2590-4420
A.R. Field https://orcid.org/0000-0003-0671-9668
L. Frassinetti https://orcid.org/0000-0002-9546-4494
S. Henderson https://orcid.org/0000-0002-8886-1256
K. Imada https://orcid.org/0000-0002-8128-2438
A. Kirk https://orcid.org/0000-0002-5746-6595
T. Luda https://orcid.org/0000-0002-9941-0039
S.F. Smith https://orcid.org/0000-0003-2319-0356

References

[1] Dimits A.M., Williams T.J., Byers J.A. and Cohen B.I. 1996 *Phys. Rev. Lett.* **77** 71–74
[2] Kinsey J.E., Staebler G.M., Candy J., Waltz R.E. and Budny R.V. 2011 *Nucl. Fusion* **51** 083001
[3] Nuttall W., Konishi S., Takeda S. and Webbe-Wood D. 2020 *Commercialising Fusion Energy* (IOP Publishing Ltd)
[4] Snyder P.B., Groebner R.J., Leonard A.W., Osborne T.H. and Wilson H.R. 2009 *Phys. Plasmas* **16** 1–9
[5] Snyder P.B., Groebner R.J., Hughes J.W., Osborne T.H., Beurskens M., Leonard A.W., Wilson H.R. and Xu X.Q. 2011 *Nucl. Fusion* **51** 103016
[6] Saarelma S., Connor J.W., Bilkova P., Bohm P., Field A.R., Frassinetti L., Fridstrom R. and Kirk A. 2023 *Nucl. Fusion* **63** 052002
[7] Frassinetti L. *et al* 2021 *Nucl. Fusion* **61** 016001
[8] Groebner R.J., Mahdavi M.A., Leonard A.W., Osborne T.H., Wolf N.S., Porter G.D., Stangeby P.C., Brooks N.S., Colchin R.J. and Owen L.W. 2004 *Nucl. Fusion* **44** 204–13
[9] Mahdavi M.A., Maingi R., Groebner R.J., Leonard A.W., Osborne T.H. and Porter G. 2003 *Phys. Plasmas* **10** 3984–91
[10] Burrell K.H. 2003 *Phys. Plasmas* **10** 2616–8
[11] Connor F.W. 1977 *Plasma Phys.* **19** 853–73
[12] Summers H.P., Dickson W.J., O'Mullane M.G., Badnell N.R., Whiteford A.D., Brooks D.H., Lang J., Loch S.D. and Griffin D.C. 2006 *Plasma Phys. Control. Fusion* **48** 263–93
[13] Groebner R.J., Mahdavi M.A., Leonard A.W., Osborne T.H., Porter G.D., Colchin R.J. and Owen L.W. 2002 *Phys. Plasmas* **9** 2134–40
[14] Rosenthal A.M., Hughes J.W., Laggner F.M., Odstrčil T., Bortolon A., Wilks T.M. and Sciortino F. 2023 *Nucl. Fusion* **63** 042002
[15] Guttenfelder W., Groebner R.J., Canik J.M., Grierson B.A., Belli E.A. and Candy J. 2021 *Nucl. Fusion* **61** 056005
[16] Chapman-Oplopoiou B. *et al* 2022 *Nucl. Fusion* **62** 086028
[17] Kallenbach A., Asakura N., Kirk A., Korotkov A., Mahdavi M.A., Mossessian D. and Porter G.D. 2005 *J. Nucl. Mater.* **337–9** 381–5
[18] Kallenbach A., Bernert M., Dux R., Eich T., Henderson S.S., Pütterich T., Reimold F., Rohde V. and Sun H.J. 2019 *Nucl. Mater. Energy* **18** 166–74
[19] Saarelma S., Frassinetti L., Bilkova P., Challis C.D., Chankin A., Fridström R., Garzotti L., Horvath L. and Maggi C.F. 2019 *Phys. Plasmas* **26** 072501
[20] Field A.R., Chapman-Oplopoiou B., Connor J.W., Frassinetti L., Hatch D.R., Roach C.M. and Saarelma S. 2023 *Phil. Trans. R. Soc.* A **381** 20210228
[21] Luda T. *et al* (The ASDEX Upgrade Team and The Eurofusion MST1 Team) 2021 *Nucl. Fusion* **61** 126048
[22] Dunne M.G. *et al* 2017 *Plasma Phys. Control. Fusion* **59** 025010
[23] Schuster C.U. *et al* 2022 *Nucl. Fusion* **62** 066035
[24] Scannell R., Walsh M.J., Dunstan M.R., Figueiredo J., Naylor G., O'Gorman T., Shibaev S., Gibson K.J. and Wilson H. 2010 *Rev. Sci. Instrum.* **81** 045107
[25] Smith S.F., Kirk A., Chapman-Oplopoiou B., Clark J.G., Ham C.J., Horvath L., Maggi C.F., Scannell R. and Saarelma S. 2022 *Plasma Phys. Control. Fusion* **64** 045024
[26] Kotschenreuther M. *et al* 2019 *Nucl. Fusion* **59** 096001
[27] Simpson J., Moulton D., Giroud C., Groth M. and Corrigan G. 2019 *Nucl. Mater. Energy* **20** 100599
[28] Luda T., Angioni C., Dunne M.G., Fable E., Kallenbach A., Bonanomi N., Schneider P.A., Siccinio M. and Tardini G. 2020 *Nucl. Fusion* **60** 036023
[29] Luda T. *et al* 2023 *Plasma Phys. Control. Fusion* **65** 034001
[30] Giroud C. *et al* 2015 *Plasma Phys. Control. Fusion* **57** 035004
[31] Lore J.D., Bonnin X., Park J.S., Pitts R.A. and Stangeby P.C. 2022 *Nucl. Fusion* **62** 106017
[32] Maggi C.F. *et al* 2018 *Plasma Phys. Control. Fusion* **60** 14045
[33] Horvath L. *et al* 2021 *Nucl. Fusion* **61** 046015
[34] Schneider P.A. *et al* 2023 *Nucl. Fusion* **63** 112010
[35] Frassinetti L. *et al* (JET Contributors) 2023 *Nucl. Fusion Nucl. Fusion* **63** 112009
[36] Predebon I., Hatch D., Frassinetti L., Horvath L., Saarelma S., Chapman-Oplopoiou B., Görler T. and Maggi C. 2023 *Nucl. Fusion* **63** 036010
[37] Tholerus E. *et al* (the STEP Team) 2024 Flat-top plasma operational space of the STEP power plant *Nucl. Fusion* submitted